Strojniški vestnik - Journal of Mechanical Engineering 70(2024)9-10, 417-425
DOI:10.5545/sv-jme.2024.1037
Original Scientific Paper
Received for review: 2024-05-13
Received revised form: 2024-09-04
Accepted for publication: 2024-09-10

Through-thickness Work Hardening Variation in Thick High Strength Steel Plates: A Novel Inverse Characterization Method

Kristof Denys[1] – Niels Vancraeynest[1] – Steven Cooreman[2] – Marco Rossi[3] – Sam Coppieters[1,*]

[1]KU Leuven, Department of Materials Engineering, Belgium
[2]ArcelorMittal Global R&D / OCAS NV, Belgium
[3]Universitá Politecnica delle Marche, Department of Industrial Engineering and Mathematical Sciences, Italy

Due to the production process, thick high strength steel plates potentially exhibit inhomogeneous plastic material behavior through the thickness. For example, the initial yield stress and work hardening behavior might vary through the plate thickness. In order to establish a reliable plasticity model that can be used in finite element simulations to optimize forming processes or to investigate the structural integrity of large structures, this material behavior needs to be characterized. A straightforward characterization method consists of slicing the thick high strength steel plate and conducting standard tensile tests. However, this approach comes with a large experimental effort. A novel specimen is proposed enabling to inversely identify the work hardening behavior at distinct locations through the thickness of a thick steel plate. To this end, a tensile specimen with circular pockets at different depths is used. The strain fields within the pockets are captured using digital image correlation (DIC). finite element model updating (FEMU) is used to inversely identify a predefined strain hardening law for each pocket. First, the procedure is optimized and numerically verified using virtual experiments generated by a finite element model with a known variation of the work hardening behavior. Finally, the procedure is experimentally validated by characterizing the strain hardening behavior of a 10 mm thick S690QL grade.

Keywords: through thickness strain hardening, FEMU, Nelder-Mead, stereo-DIC, S690QL, thick high strength steel

Highlights

- *The variation in work hardening behavior over the thickness was measured for S690QL by slicing a conventional dog bone specimen.*
- *A novel specimen was proposed for simultaneously identifying the strain hardening behavior of five different layers in a 10 mm thick steel plate.*
- *Stereo-DIC was combined with an inverse identification scheme to identify the variation in hardening behavior for S690QL.*
- *The effect of plastic anisotropy was investigated on the proposed specimen.*

0 INTRODUCTION

Steelmaking involves a series of heating and cooling steps. During the cooling process of thick high strength steels, the outer steel solidifies faster than the inner, resulting in an inhomogeneous chemical composition and microstructure through the thickness of the steel [1] and [2]. For example, Nanba et al. [1] observed a larger grain size at the mid-thickness than at the surface of hot-rolled carbon steels. Raabe [2] observed large blocks of austenitic dendrites at the surface and austenitic grain structure with a martensitic volume fraction of 20 % at the mid-thickness region of hot-rolled stainless steel. The inhomogeneous through-thickness microstructure and chemical composition potentially leads to direction-dependent mechanical properties [3] and [4], especially in the direction perpendicular to the surface, referred to as the through-thickness direction [5]. Several authors reported inhomogeneous material behavior in the through-thickness direction of thick steels [6] to [8]. Moreover, the ASTM standard notes that there might be a measurable difference in mechanical properties through the thickness [9]. In addition to steelmaking-induced inhomogeneous through-thickness material behavior, it must be noted that secondary forming processes can also induce this phenomenon. Indeed, in forming processes involving bending deformation, the outer layers are typically subjected to higher levels of strain, hence experience more work hardening than the inner layers. This can result in a gradient of plastic material behavior, e.g. strength, hardness and work hardening behavior, through the thickness of the plate. For example, during spiral forming of pipe line, the inner side is subjected to compression and the outer pipe side to tension while the mid-layer does not experience plastic deformation. This yields a gradient in the degree of work hardening resulting in different mechanical properties through the wall-thickness of the pipe line [8]. Overall, it can be stated that the degree to which work hardening varies through the thickness of a steel plate depends on several factors including the steelmaking process, the type of steel, the plate thickness and the applied secondary forming process. Finite element simulations are used to study and optimize secondary forming processes such as

*Corr. Author's Address: KU Leuven, Dept. of Materials Engineering, Ghent Campus, Gebroeders De Smetstraat 1, 9000 Gent, Belgium, sam.coppieters@kuleuven.be

spiral forming [10] of pipe line, but also to assess the structural integrity of the resulting pipe line [11]. The predictive accuracy of these simulations, however, highly depends on the accuracy of the adopted plasticity model [10] and [11]. As such, it is required to characterize the through-thickness variation of the material properties so that a reliable plasticity model can be established.

While a large literature exists for characterizing the planar behavior of sheet metal [12] to [15], the testing methods to derive the through-thickness behavior are less widespread. So-called through-thickness tensile tests can be performed on small tensile samples [6] and [16] removed from the thick plate, see Fig. 1 for a schematic of this approach. The test enables to determine the through-thickness ductility, also referred to as Z-qualities [4]. However, the feasibility of this test highly depends on the plate thickness. Indeed, the specimen needs to be manufactured without modifying the material behavior and a suitable testing machine (small specimen, yet a large load capacity is required) needs to be available. To circumvent the latter, Barsom et al. [6] proposed to weld extensions to the small tensile specimen, see Fig. 1b. However, this results in a heat affected zone potentially changing the mechanical properties in the gauge section. Furthermore, standard through-thickness tensile tests yield the average material behavior in the gauge section. Consequently, the standard test does not yield information with regard to the variation of the work hardening behavior through the thickness. Moreover, the gauge section is only a part of the full thickness. Indeed, the material near the two surfaces is used to clamp the tensile specimen or is affected by the welding of extensions. Finally, Barsom et al. [6] also concluded that the through-thickness test yields the mechanical properties of the weakest region throughout the thickness.

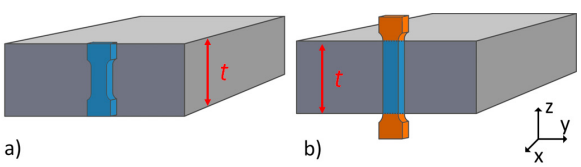

Fig. 1. *Illustration of a through thickness tensile test: a) machined from the entire thickness and b) with an extension (orange) welded onto the gauge section; the plate thickness t is indicated by the red arrows*

As opposed to the through-thickness tensile test, the indentation hardness test in the thickness direction enables to detect inhomogeneous material behavior [7]. Indeed, hardness measurements can be converted into an initial yield strength [17]. Indentation hardness measurements, however, suffer from a substantial standard deviation [18]. Moreover, indentation hardness measurements through the thickness cannot be converted in the required flow curve describing the work hardening behavior. Probably the most straightforward approach to determine the variation of work hardening behavior in the through-thickness direction, is to slice a thick tensile specimen into several thin tensile specimens and performing tensile tests as proposed by Sohn et al. [8]. This directly yields the flow curve and the associated material properties as a function of the through-thickness direction. The slicing method should be carefully selected to minimize the influence on the measured flow curves. For example, wire-cut electrical discharge machining (EDM) can be used to slice the thick high strength steel. However, EDM potentially induces heat into a specific part of the sample resulting in a heat affected zone [19]. Additionally, independent of the chosen production process, it is inevitable that during slicing a part of the material is removed and the residual stresses are partially released. These effects might have an influence on the accuracy achieved by the slicing method. The large cost associated with the production of the slices and the limited measurement accuracy are the main impetus for this work. In this work, a novel inverse characterization method for determining the work hardening variation in thick steel plates is presented. The method is devised in the context of Material Testing 2.0 (MT2.0) [20]. A full thickness tensile specimen with circular pockets at different depths is used to inversely determine the work hardening of the different material layers probed by the pockets. During the tensile test, digital image correlation (DIC) is used to measure the strain fields within the different pockets. Those strain fields are fed to a finite element model updating (FEMU) [21] to [25] code characterizing a predefined hardening law for each probed material layer. This procedure is verified in a numerical concept study using virtual experiments. Finally, the inverse procedure is experimentally validated on a S690QL steel grade with a nominal thickness of 10 mm. The obtained results are compared with the slicing method. The paper is organized as follows. In section two, the slicing method is described and the results obtained for a 10 mm thick S690QL steel are discussed. In section three, numerical simulations incorporating the observed material behavior from section two are used to design the tensile specimen with pockets at different depths. Virtual experiments generated with finite element models [26] and [27] are used to verify

the proposed FEMU method. Section four embarks on the experimental validation of the proposed method.

1 THE SLICING METHOD

To establish a benchmark for the varying strain hardening behaviours across the thickness of the 10 mm thick S690QL steel, a dog bone specimen was prepared in the transverse direction (TD) relative to the rolling direction. This specimen was then sectioned into five thin tensile samples, each with a nominal thickness of 1.8 mm, using wire electrical discharge machining. The thin tensile samples were subjected to a standard tensile test. A standard tensile machine with a load capacity of 250 kN was used. An extensometer with an initial gage length of 80 mm was used to measure the elongation. The slicing method is illustrated in Fig. 2c.

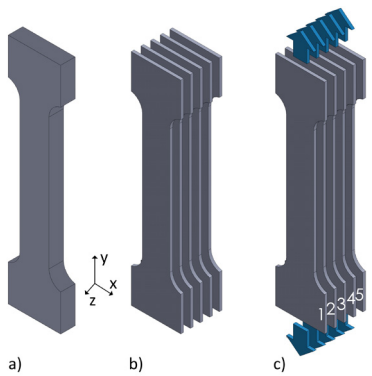

Fig. 2. *a) dog bone, b) slicing of dog bone into five layers, and c) performing a tensile test on each layer. The tensile direction (y) corresponds to the TD*

The results of the five tensile tests are shown in Fig. 3, where the true stress is plotted as a function of the equivalent plastic strain ε_{eq}^{pl}. The numbers of the slices can be found in Fig. 2 where 1 and 5 represent the outer layers. It can be inferred from Fig. 3 that outer layers (slices 1 and 5) exhibit a similar strain hardening behaviour, yet the absolute stress levels significantly differ. The difference in initial yielding (i.e. the proof stress at $\varepsilon_{eq}^{pl} = 0.002$) between the outer layers is approximately 10 %. It can be seen that the strain hardening behaviour is distinctly different between the outer layers and the inner layers. The outer layers exhibit a strain hardening behaviour that can be described by a power law equation, while the inner layers exhibit linear strain hardening. Moreover, it can be concluded that the inner layers (slices 2, 3 and 4) exhibit approximately the same strain hardening behaviour. The overall observation is that the strain hardening behaviour is not symmetrical with respect to the mid-thickness layer (slice 3), a phenomenon that has been previously reported by Raabe et al. [2].

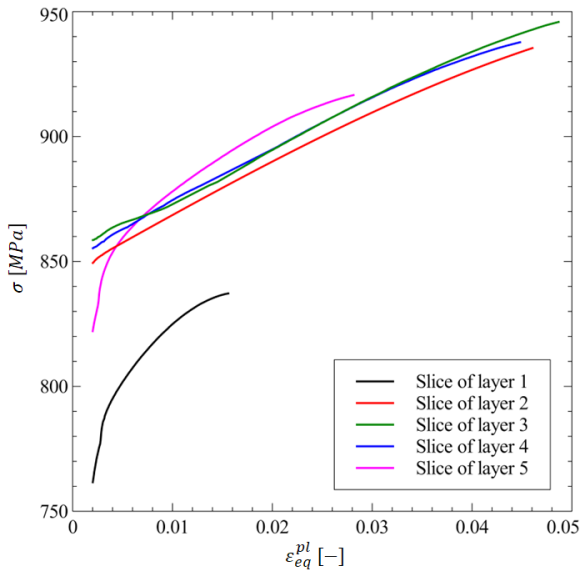

Fig. 3. *The slicing method: strain hardening behavior of five layers through the thickness, numbered as in Fig. 2; initial yielding is determined through the proof stress*

2 THE FEMU METHOD

Fig. 4 schematically shows the proposed tensile specimen with five circular pockets at different depths. The pockets are chosen in accordance with the layers tested via the slicing method presented in the previous section. The diameter D of the pockets is first optimized via three virtual experiments assuming D = 10 mm, 20 mm and 30 mm. To this end, the tensile experiments are simulated using Abaqus/Standard using a reference strain hardening behavior for each layer. The reference strain hardening behavior of the five different layers is shown in Fig. 5 by the solid lines. It can be inferred that the reference strain hardening behavior qualitatively corresponds to the strain hardening behavior determined by the slicing method, see Fig. 3, ensuring a realistic material behavior in the virtual experiments. Swift's hardening law is used to describe the strain hardening of each individual layer. The von Mises yield criterion is used to simulate the three tensile tests using the reference hardening behavior shown in Fig. 5. The virtual test data generated by the FE models is then used to verify the FEMU code, hence determining the optimal diameter D. It must be noted that the FEMU

code simultaneously identifies fifteen unknown strain hardening parameters (five layers, each layer is described by Swift's hardening law with three model parameters). To limit the computational cost, the adaptive Nelder-Mead simplex method **[28]** has been employed to inversely identify the sought parameters. The FEMU code essentially minimizes the discrepancy between the numerical and experimental strain fields within the pockets, i.e. the blue regions in Fig. 4.

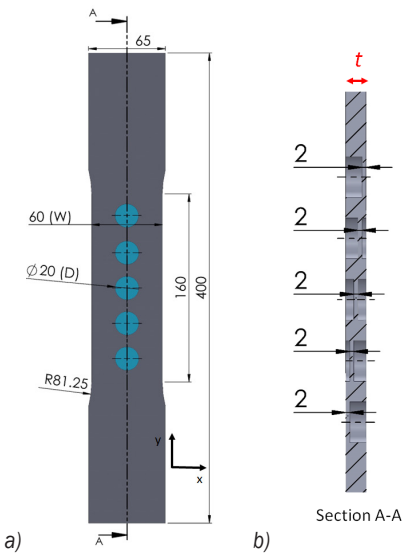

Fig. 4. *a) Front view of the full thickness tensile specimen with five circular pockets at different depths, and b) geometry of the pockets shown through Section A-A with t the thickness of the plate*

In the virtual experiments, the experimental strain fields are obtained from the simulation using the reference strain hardening. In practice, the experimental strain fields are acquired by stereo-DIC measurements. Because the FE simulation is displacement-driven, also the tensile force F can be considered. The surface strains components (ε_{xx}, ε_{yy} and ε_{xy}) and tensile force F have a different order of magnitude. To obtain an equal weight in the cost function $C(\mathbf{p})$, the strain components and the tensile force have been normalized by their root mean square (RMS) value and experimental tensile force, respectively:

$$C(\mathbf{p}) = \sum_{i=1}^{m}\sum_{j=1}^{n_i}\left[\left(\frac{\varepsilon_{xx,ij}^{exp}-\varepsilon_{xx,ij}^{num}}{\varepsilon_{xx,RMS,i}^{exp}}\right)^2+\left(\frac{\varepsilon_{yy,ij}^{exp}-\varepsilon_{yy,ij}^{num}}{\varepsilon_{yy,RMS,i}^{exp}}\right)^2 + \left(\frac{\varepsilon_{xy,ij}^{exp}-\varepsilon_{xy,ij}^{num}}{\varepsilon_{xy,RMS,i}^{exp}}\right)^2\right] + \sum_{i=1}^{m}\left[n_i\left(\frac{F_i^{exp}-F_i^{num}}{F_i^{exp}}\right)^2\right]. \quad (1)$$

with $\mathbf{p}$ the vector of the unknown parameters of Swift's hardening models, m the number of load steps (five in this study) and n_i the number of data points from the DIC measurement at load step i. The subscripts exp and num represent the experimental and numerical response, respectively. The results of the virtual experiments for D = 10 mm, 20 mm and 30 mm are shown in Figs. 5a, b and c, respectively. The reference strain hardening behavior is shown by the solid lines, the inversely identified strain hardening is shown by the circles. Each color represents the same material layer. Clearly, the size of the diameter affects the robustness and accuracy of the identification. It can be observed that the specimen with a diameter of D = 20 mm enables an accurate inverse identification. The results suggest that the identifiability decreases for a diameter larger than D = 20 mm, probably because of the interaction between the pockets. The results for D = 10 mm are good, yet from an experimental point of view it is deemed more suited to opt for the largest suitable diameter. Indeed, a larger pocket diameter enhances the application of a speckle pattern and ensures adequate measurement resolution.

3 EXPERIMENTAL VALIDATION AND DISCUSSION

The sample is manufactured by precision milling using extensive cooling to avoid surface hardening. The quasi-static experiment is conducted on a MTS tensile machine with a load capacity of 1000 kN equipped with hydraulic wedge grips. One stereo-DIC setup was used to acquire the five strain fields within the pockets. The adopted DIC settings can be found in Appendix, see Table 1. The experimental setup is shown in Fig. 6. The FEMU code was employed to simultaneously identify five independent, yet identical strain hardening models as Swift's hardening law is assumed for each layer. The initial guess for the hardening behavior of each layer is taken from a tensile test on the full thickness. The initial guess for the hardening behavior is shown by the dashed black line in Fig. 7. The inversely identified hardening behavior is shown in Fig. 7 by the circles. The solid lines represent the measured strain hardening behavior obtained from the slicing method in Section 1. Each color represents the same material layer. It can be observed that the inversely identified strain hardening (circles) does not perfectly match the results from the slicing method (solid lines). However, it can be clearly observed that the FEMU code identified a substantially lower strain hardening behaviour for Layer 1. This trend is in good agreement with the variation of strain hardening found by the slicing

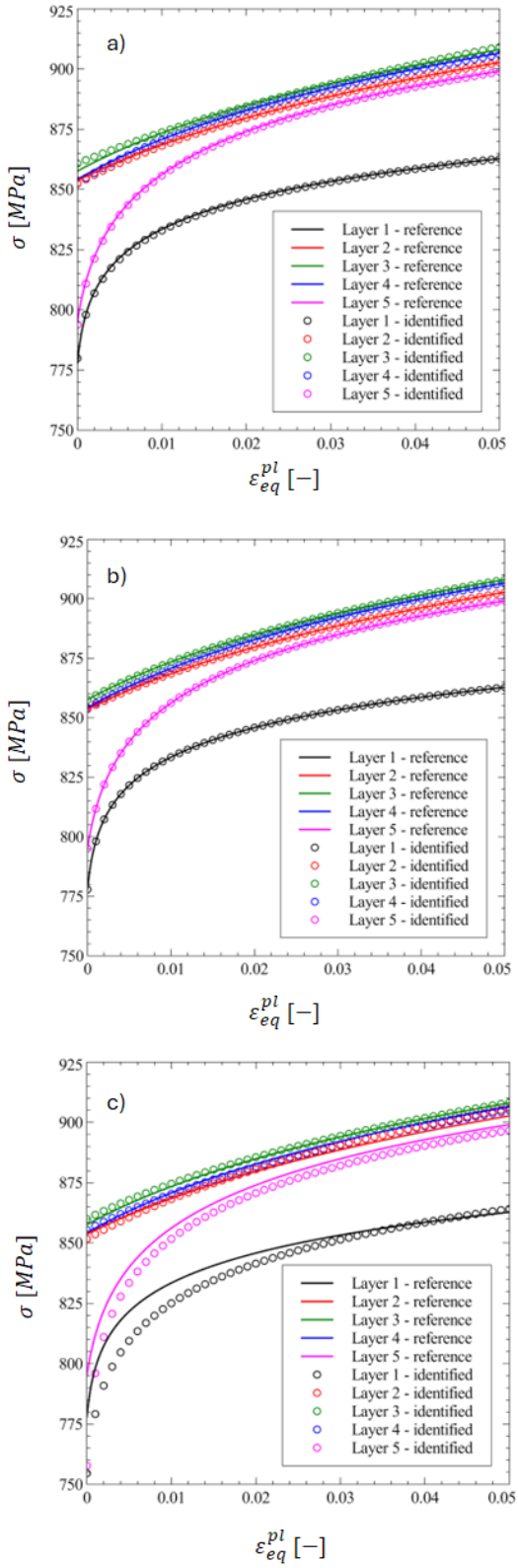

Fig. 5. *Numerical verification of the FEMU method; reference (solid lines) and inversely identified (symbols) flow curves obtained with a) D = 10 mm, b) D = 20 mm and c) D = 30 mm*

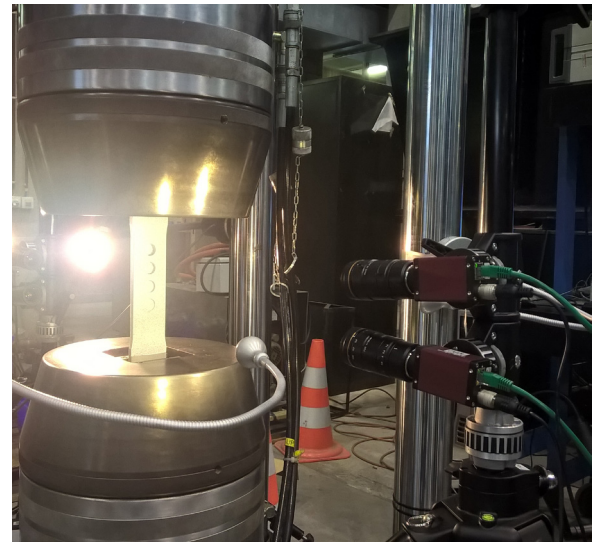

Fig. 6. *Setup of the tensile test with a stereo-DIC measurement*

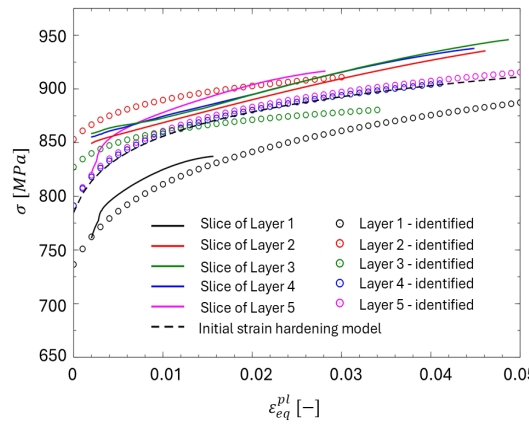

Fig. 7. *Comparison between the through-thickness flow curves identified through the slicing method and the FEMU method*

method. The observed discrepancy between the slicing method and the FEMU method are potentially attributed to:

- The predefined character of Swift's hardening law. A general downside of the current FEMU code is that a hardening law is used to parameterize the strain hardening behavior. If the adopted hardening law cannot describe the actual strain hardening of a particular layer, the identification of the other layers will be biased. For example, Fig. 7 shows that the slicing method yields linear strain hardening for Layers 2, 3 and 4. Such linear strain hardening cannot be described by Swift's hardening law, hence potentially affects the identification accuracy of the outer layers. A multi-linear strain hardening

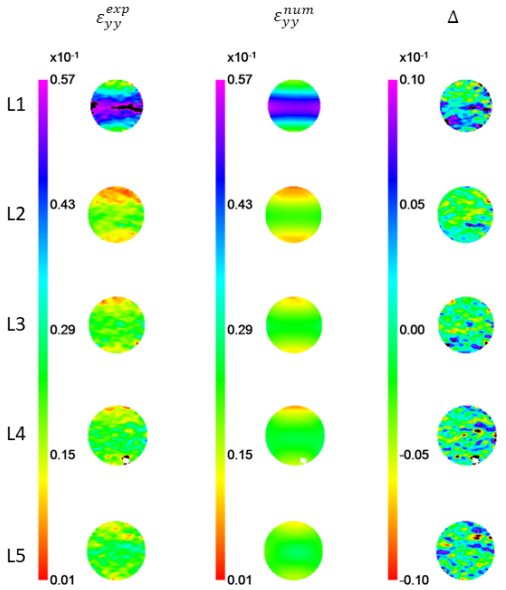

Fig. 8. *Comparison of the experimentally and numerically obtained longitudinal strains: Layer 1 (L1) to Layer 5 (L5)*

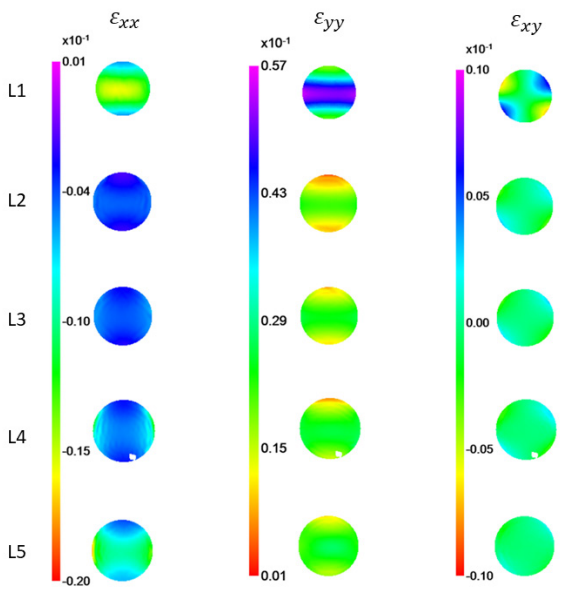

Fig. 9. *Numerically predicted strain fields using the inversely identified flow curves: Layer 1 (L1) to Layer 5 (L5)*

model would eliminate the problem yet might introduce robustness problems as reported by Denys et al. [29].

- The slicing method used specimens with a thickness of approximately 1.8 mm, the FEMU method considers layers of 2 mm in each pocket.
- The slicing method removes the residual stress between the different layers that, instead, is still present in the material surrounding the circular holes in the FEMU method.
- The FEMU method assumes that the material is plastically isotropic. However, the material potentially exhibits plastic anisotropy which could bias the identification.

It is assumed that the difference in sheet thickness between the slicing method and the FEMU method will have marginal effect. Indeed, while the strain hardening variation is pronounced over a 10 mm thickness, it is questionable whether such differences would be observable over a much smaller range of just 0.2 mm using the FEMU method. The effect of plastic anisotropy is further investigated in the remainder of this section. Fig. 8 shows the numerically predicted and the experimentally measured strain fields (the longitudinal strain ε_{yy} is shown) in the five pockets. It can be inferred that the experimental and the numerical strain fields qualitatively correspond, the value of the difference between the two strain fields Δ is also shown. From Fig. 8 each pocket exhibits a different strain field. Moreover, the strain field within each pocket is inhomogeneous. The inhomogeneity of the strain field within each pocket is shown in

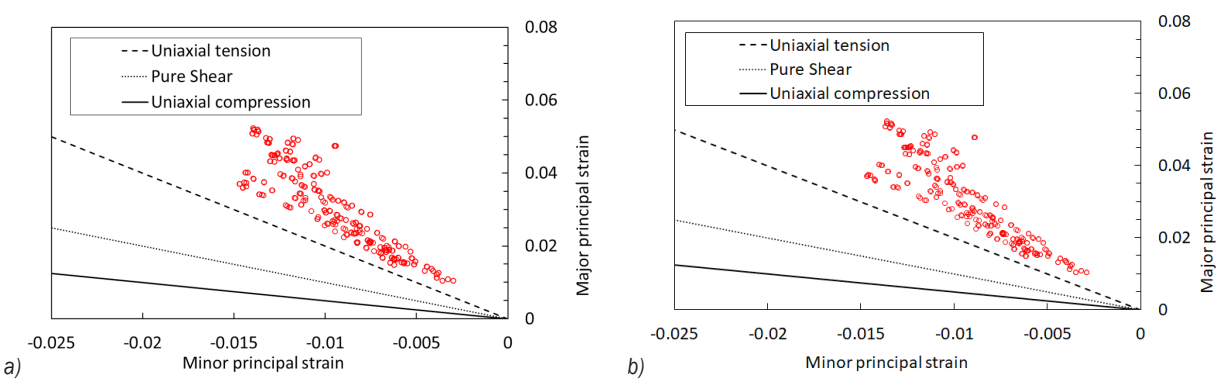

Fig. 10. *Comparison of the strain state in layer 5 predicted at the final load step by: a) von Mises, and b) Hill48*

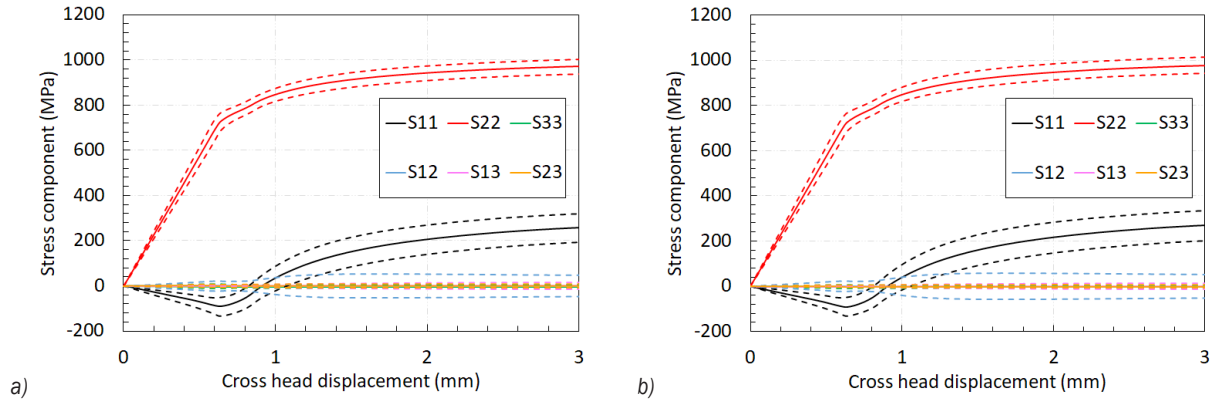

Fig. 11. *Comparison the stress state evolution in Layer 5 predicted by: a) von Mises, and b) Hill48*

detail in Fig. 9. This figure shows the in-plane strain components computed using the inversely identified flow curves and the results confirm that in all pockets an inhomogeneous strain state prevails. Consequently, layers within the pockets are subjected to a multi-axial stress state. The thin circular layer deforms in accordance with the surrounding thick material. The circular pocket elongates and contracts, hence forming an ellipse. This deformation is imposed to the thin layer resulting in a multi-axial stress state.

Fig. 10a shows the strain state in Layer 5 at the final load step. It can be inferred that the majority of the material points deviate from uniaxial tension. A similar strain state is found for all layers. Fig. 11a shows the evolution of the mean stress components in Layer 5. The dashed lines represent one standard deviation. First, it can be concluded that plane stress conditions prevail in the layer since the out-of-plane stress components (S33, S13 and S23) are zero. Second, most of the points is subjected to biaxial tension after the onset of yielding, hence plastic anisotropy might play a role of importance in the inverse identification. Indeed, by selecting the von Mises criterion in the inverse identification, it was implicitly assumed that an increase in the cost function caused by an error in the work hardening is significantly larger than an increase caused by an error in the anisotropic yield function. To assess the importance of plastic anisotropy, the strain and stress state analysis was repeated using the 3D Hill48 yield criterion. The anisotropy parameters were calibrated in **[30]** and the values can be found in Appendix, see Table 2. It should be emphasized that it is assumed that the plastic anisotropy does not vary through the thickness of the plate. Fig. 10b and Fig. 11b show the strain state and mean stress evolution in layer 5 considering the plastic anisotropy of S690QL, respectively. When comparing these results with Fig. 10a and Fig. 11a, it can be concluded that plastic anisotropy does not play a significant role in this material and can be neglected. Indeed, it can be inferred from Table 2 that the investigated material exhibits a relatively weak plastic anisotropy.

4 CONCLUSIONS

A FEMU-based method is proposed to characterize the inhomogeneous through-thickness strain hardening behavior of thick steel plate. The procedure relies on a full thickness tensile specimen with circular pockets at different depths enabling to probe work hardening in different layers through the thickness. During the tensile test, the strain fields within the pockets are measured using digital image correlation. The strain fields are then fed to a FEMU code which inversely identifies the strain hardening behavior defined in the finite element model. The identification procedure is first optimized and verified using virtual experiments. Subsequently, experimental validation is pursued by applying the procedure to a sample of S690QL grade, which has a thickness of 10 mm. Based on these investigations, the following conclusions can be drawn:

- The proposed inverse method enables to simultaneously identify the strain hardening behavior of five different layers in a 10 mm thick steel plate.
- The inverse identification process demonstrates qualitative agreement with the slicing method. However, a slight discrepancy is observed, which can primarily be attributed to the predefined nature of the hardening law in the FEMU method.
- S690QL displays a notable variation in work hardening behavior across its thickness.

5 APPENDIX

Table 1. *Specification of the DIC parameters for stereo-DIC set front*

DIC implementation	Specification
Matching criteria	ZNSSD
Interpolation	Bicubic interpolation
Transformation	Affine
Subset	21 pixels
Step	1 pixel
Displacement resolution	$1.49 \cdot 10^{-3}$ mm
Strain smoothing	Bilinear interpolation
Strain window size	7 Datum points
Strain resolution	$3.28 \cdot 10^{-3}$

Table 2. *Anisotropy parameters of the 3D Hill48 yield criterion for S690QL (10 mm)*

F	G	H	N	M	L
0.485	0.481	0.519	1.445	1.741	1.352

6 ACKNOWLEDGEMENTS

The authors gratefully acknowledge the support from the Research Fund for Coal and Steel under grant agreement No 888153 (EU-RFCS 2019 project No. 888153 | vForm-xSteels).

7 DISCLAIMER

The results reflect only the authors' view, and the European Commission is not responsible for any use that may be made of the information it contains.

8 REFERENCES

[1] Nanba, S., Kitamura, M., Shimada, M., Katsumata, M., Inoue, T., Imamura, H., Maeda, Y., Hattori, S. (1992). Prediction of Microstructure Distribution in the Through-thickness Direction during and after Hot Rolling in Carbon Steels. *ISIJ International*, vol. 32, no. 3, p. 377-386, **DOI:10.2355/isijinternational.32.377**.

[2] Raabe, D. (1995). Textures of strip cast and hot rolled ferritic and austenitic stainless steel. Material Science and Techology, vol. 11, no. 5, p. 461-468, **DOI:10.1179/mst.1995.11.5.461**.

[3] ISO 7778:2024. *Through-Thickness Characteristics for Steel Products*, International Standard Organization, Geneva.

[4] EN 10164 (2004). *Steel Products with Improved Deformation Properties Perpendicular to the Surface of the Product - Technical Delivery Conditions*, Europäischen Normen, Berlin.

[5] Gervasyev, A., Petrov, R., Pyshmintsev, I., Struin, A., Leis, B. (2016). Mechanical properties anisotropy in ×80 line pipes. *ASME Proceedings of the 11th International Pipeline Conference*, p. 26-30, **DOI:10.1115/IPC2016-64695**.

[6] Barsom, J.M., Korvink, S.A. (1998). Through-Thickness Properties of Structural Steels. *Journal of Structural Engineering*, vol. 124, no. 7, **DOI:10.1061/(ASCE)0733-9445(1998)124:7(727)**.

[7] Xu, P., Yin, F., Nagai, K. (2004). The thickness gradient of microstructure and mechanical property in an as-cast thin steel slab. *Materials Transactions*, vol. 45, no. 7, p. 2456-2462, **DOI:10.2320/matertrans.45.2456**.

[8] Sohn, S.S., Han, S.Y., Bae, J., Kim, H.S., Lee, S. (2013). Effects of microstructure and pipe forming strain on yield strength before and after spiral pipe forming of API X70 and X80 linepipe steel sheets. *Materials Science and Engineering: A*, vol. 573, p. 18-26, **DOI:10.1016/j.msea.2013.02.050**.

[9] ASTM A20/A20M-2014. *Standard Specification for General Requirements for Steel Plates for Pressure Vessels*, ASTM International, West Conshohocken.

[10] Cooreman, S., Thibaux, P., Liebeherr, M. (2018). Prediction of mechanical properties on large diameter welded pipes through advanced constitutive modelling. *Journal of Physics: Conference Series*, vol. 1063, 012043, **DOI:10.1088/1742-6596/1063/1/012043**.

[11] Paermentier, B., Cooreman, S., Verleysen, P., Chandran, S., Coppieters, S., Talemi, R. (2022). A dynamic tensile Tear test methodology to characterise dynamic fracture behaviour of modern High-Grade pipeline steels. *Engineering Fracture Mechanics*, vol. 272, 108687, **DOI:10.1016/j.engfracmech.2022.108687**.

[12] Vrh, M., Halilovič, M., Štok, B. (2008). Impact of Young's modulus degradation on springback calculation in steel sheet drawing. *Strojniški vestnik - Journal of Mechanical Engineering*, vol. 54, no. 4, p. 288-296.

[13] Starman, B., Vrh, M., Halilovič, M., and Štok, B. (2014). Advanced modelling of sheet metal forming considering anisotropy and Young's modulus evolution. *Strojniški vestnik - Journal of Mechanical Engineering*, vol. 60, no. 2 p. 84-92. **DOI:10.5545/sv-jme.2013.1349**.

[14] Starman, B., Vrh, M., Koc, P., Halilovič, M. (2019). Shear test-based identification of hardening behaviour of stainless steel sheet after onset of necking. *Journal of Materials Processing Technology*, vol. 270 p. 335-344, **DOI:10.1016/j.jmatprotec.2019.03.010**.

[15] Rossi, M. Lattanzi, A., Morichelli, L., Martins, J.M.P., Thuillier, S., Andrade-Campos, A., Sam Coppieters, S. (2022). Testing methodologies for the calibration of advanced plasticity models for sheet metals: A review. *Strain*, vol. 58, no. 6, e12426, **DOI:10.1111/str.12426**.

[16] Wang, Y.-Q., Liao, X.-W., Zhang, Y.-Y., Shi, Y.-J. (2015). Experimental study on the through-thickness properties of structural steel thick plate and its heat-affected zone at low temperatures. *Journal of Zhejiang University-SCIENCE A*, vol. 16 p. 217-228, **DOI:10.1631/jzus.A1400273**.

[17] Cahoon, J.R., Broughton, W.H., Kutzak, A.R. (1971). The determination of yield strength from hardness measurements. *Metallurgical Transactinons*, vol. 2, p. 1979-1983, **DOI:10.1007/BF02913433**.

[18] Pavlina, E.J, Van Tyne, C.V. (2008). Correlation of yield strength and tensile strength with hardness for steels. *Journal of Materials Engineering and Performance*, vol. 17, p. 888-893, **DOI:10.1007/s11665-008-9225-5**.

[19] Lee, L.C., Lim, L.C., Narayanan, V., Venkatesh, V.C. (1988). Quantification of surface damage of tool steels after EDM. *International Journal of Machine Tools and Manufacturing*, vol. 28, no. 4, p. 359-372, **DOI:10.1016/0890-6955(88)90050-8**.

[20] Pierron, F., Grédiac, M. (2021). Towards Material Testing 2.0. A review of test design for identification of constitutive parameters from full-field measurements. *Strain*, vol. 57, e12370, **DOI:10.1111/str.12370**.

[21] Avril, S. Bonnet, M., Bretelle, A.S., Grédiac, M., Hild. F., Ienny, P., Latourte, F., Lemosse, D., Pagani, S., Pagnacco, E., Pierron, F. (2008). Overview of identification methods of mechanical parameters based on full-field measurements. *Experimental Mechanics*, vol. 48, p- 381-402, **DOI:10.1007/s11340-008-9148-y**.

[22] Cooreman, S. (2008). *Identification of The Plastic Material Behaviour Through Full-Field Displacement Measurements and Inverse Methods*, PhD thesis, University of Brussels, Brussels.

[23] Denys, K., Coppieters, S., Seefeldt, M., Debruyne, D. (2016). Multi-DIC setup for the identification of a 3D anisotropic yield surface of thick high strength steel using a double perforated specimen. *Mechanics of Materials*, vol. 100,p. 96-108, **DOI:10.1016/j.mechmat.2016.06.011**.

[24] Maček, A., Urevc, J., Halilovič, M. (2021). Flat specimen shape recognition based on full-field optical measurements and registration using mapping error minimization method. *Strojniški vesnik - Journal of Mechanical Engineering*, vol. 67, no. 5, p. 203-213, **DOI:10.5545/sv-jme.2021.7111**.

[25] Maček, A., Urevc, J., Žagar, T., Halilovič, M. (2021). Crimp joint with low sensitivity to process parameters: numerical and experimental study. *International Journal of Material Forming*, vol. 14 p. 1233-1241, **DOI:10.1007/s12289-021-01637-5**.

[26] Rossi, M., Lava, P., Pierron, F., Debruyne, D., Sasso, M. (2015). Effect of DIC spatial resolution, noise and interpolation error on identification results with the VFM. Strain, vol. 51, no. 3, p. 206-222, **DOI:10.1111/str.12134**.

[27] Badaloni, M., Rossi, M., Chiappini, G., Lava, P., Debruyne, D. (2015). Impact of experimental uncertainties on the identification of mechanical material properties using DIC. *Experimental Mechanics*, vol. 55, p. 1411-1426, **DOI:10.1007/s11340-015-0039-8**.

[28] Gao, F., Han, L.(2012). Implementing the Nelder-Mead simplex algorithm with adaptive parameters. *Computational Optimization and Applications*, vol. 51, p. 259-277, **DOI:10.1007/s10589-010-9329-3**.

[29] Denys, K., Coppieters, S., Debruyne, D. (2018). On the identification of a high-resolution multi-linear post-necking strain hardening model. *Comptes Rendus Mécanique*, vol. 346, no. 8, p. 712-723, **DOI:10.1016/j.crme.2018.06.002**.

[30] Denys, K. (2017). *Investigation into the Plastic Material Behaviour up to Fracture of thick HSS Using Multi-DIC and FEMU*. PhD Thesis, KU Leuven, Leuven.